Engineering a ratiometric fluorescent sensor membrane containing carbon dots for efficient fluoride detection and removal

Meng Li[a,b*], Xiaoning Li[a,b], Mingyue Jiang[c], Xue Liu[c], Zhijun Chen[c*], Sabrina Wang[d], Tony D. James[d], Lidong Wang[a,b], Huining Xiao[e]

[a] *Hebei Key Lab of Power Plant Flue Gas Multi-Pollutants Control, Department of Environmental Science and Engineering, North China Electric Power University, Baoding, 071003, PR China*

[b] *MOE Key Laboratory of Resources and Environmental Systems Optimization, College of Environmental Science and Engineering, North China Electric Power University, Beijing, 102206, PR China*

[c] *Key Laboratory of Bio-based Material Science and Technology of Ministry of Education, Material Science and Engineering College, Northeast Forestry University, Hexing Road 26, Harbin 150040, P.R. China*

[d] *Department of Chemistry, University of Bath, Bath, BA2 7AY, UK*

[e] *Department of Chemical Engineering and Limerick Pulp & Paper Centre, University of New Brunswick, 15 Dineen Drive, Fredericton NB E3B 5A3, Canada*

Corresponding Author

*Meng Li, E-email: mlincepu@hotmail.com

*Zhijun Chen, E-mail: chenzhijun@nefu.edu.cn

Abstract

Fluoride anion pollution is one of the main problems that needs to be addressed in contaminated water. Herein, we have developed a novel sensing platform using a pyrene boronic acid and carbon dots (CDs) for the selective detection and removal of fluoride (F^-) ion at environmentally relevant levels. The probe consists of pyrene-boronic acid (PyB) moieties immobilized on to the surface of water-soluble CDs. The pyrene-boronic acid-based CDs (CDs-PyB) result in a sensor whose response in linear for F^- concentrations over a range from 0-200 μM ($R^2 = 0.996$) with a detection limit of 5.9×10^{-5} M and displays high selectivity for F^- over other anions. In addition, an amino-modified cellulose membrane containing CDs-PyB has been prepared for practical sensing and removal of F^-. The cellulose membrane-based sensor shows great potential for the detection of F^- with a high sensitivity, and excellent F^- adsorption and removal efficiency of 90.2%. Moreover, an MTT assay for the membrane demonstrates high cell proliferation ca 400% after 5 days culture, indicating excellent cytocompatibility. Our approach offers a promising direction for the construction of other sensors by simply swapping the current probe with suitable replacements for a variety of relevant applications using biocompatible and abundant naturally based materials.

Keywords: Boronic acid; Carbon dots; Ratiometric fluorescent sensor; Fluoride detection and removal; Cytocompatibility

1. Introduction

The development of fluorescent membranes capable of rapidly detecting and removing fluoride (F^-) in wastewater has received significant attention due to the toxicity of F^- [1, 2]. High levels of F^- in drinking water can cause both dental and skeletal fluorosis [3]. Based on World Health Organization (WHO) guidelines, the detection levels of F^- in drinking water should be below 1.5 ppm [4]. Therefore, methods for highly sensitive and selective detection and removal of F^- ions are urgently required [5]. Amongst the various methods of F^- recognition, boronic acid based fluorescent probes are extensively employed due to the distinct nature of the boronic acid-fluoride binding and the intrinsic selectivity against other anions [6-9]. However, conventional boronic acid based fluorescent molecules easily aggregate in aqueous media resulting in undesirable aggregation-induced quenching (ACQ), in addition this makes it difficult to fabricate fluorescent responsive membrane device [10-13]. Thus functionalisation of the probe molecules with an material support, such as nanomaterials, has been employed for establishing an anti-aggregation-caused quenching (AACQ) system [14, 15].

While the introduction of the material support could solve the above problem, most AACQ sensing systems exhibit a single fluorescence signal, which could compromise their sensing efficiency [16, 17]. Fluorescence resonance energy transfer (FRET) design is a well-established strategy, where the ratio of a dual response system can eliminate background interference and thus greatly improve sensitivity [18-24]. Therefore, fluorescent carbon dots (CDs) synthesized from biomass have attracted

much attention owing to the good water solubility, biocompatibility and high photostability [25-27]. The fluorescent CDs could be employed as both a solid support and an energy acceptor due to their tunable emission [28, 29]. Meanwhile, the introduction of CDs could greatly enhance the solubility of the organic probe molecules for aqueous F^- detection [30, 31].

Moreover, cellulose based membranes, especially the amino-modified cellulose membrane, have been widely employed for the adsorption of anions [32, 33]. Compared to some polymer membranes [34, 35], cellulose membranes are suitable for environmental applications owing to their biodegradable properties [36, 37]. As such cellulose based fluorescent membranes have been used for F^- sensing [38]. However, only a few fluorescent membranes with both AACQ and FRET effect have been developed for the detection and removal of F^- [39, 40]. These materials will significantly promote sensing and purification technologies for real world applications [41, 42].

Herein, we describe a ratiometric F^- nanosensor using PyB as the energy donor and CDs as energy acceptor and support (Scheme 1). Particularly, the affinity of a boron atom toward F^- represents an attractive approach due to the excellent selectivity and sensitivity for F^-. The nanosensor displays high sensitivity for F^- and good selectivity over other anions employed in this study. Furthermore, the nanosensor could be processed as a precursor for an amino-modified cellulose membrane-based sensor for the detection and removal of F^-. The material reported in this work exhibits high

technological potential, because apart from the rapid sensing and scavenging of F^-, it is of biological origin and as such is recyclable and biocompatible.

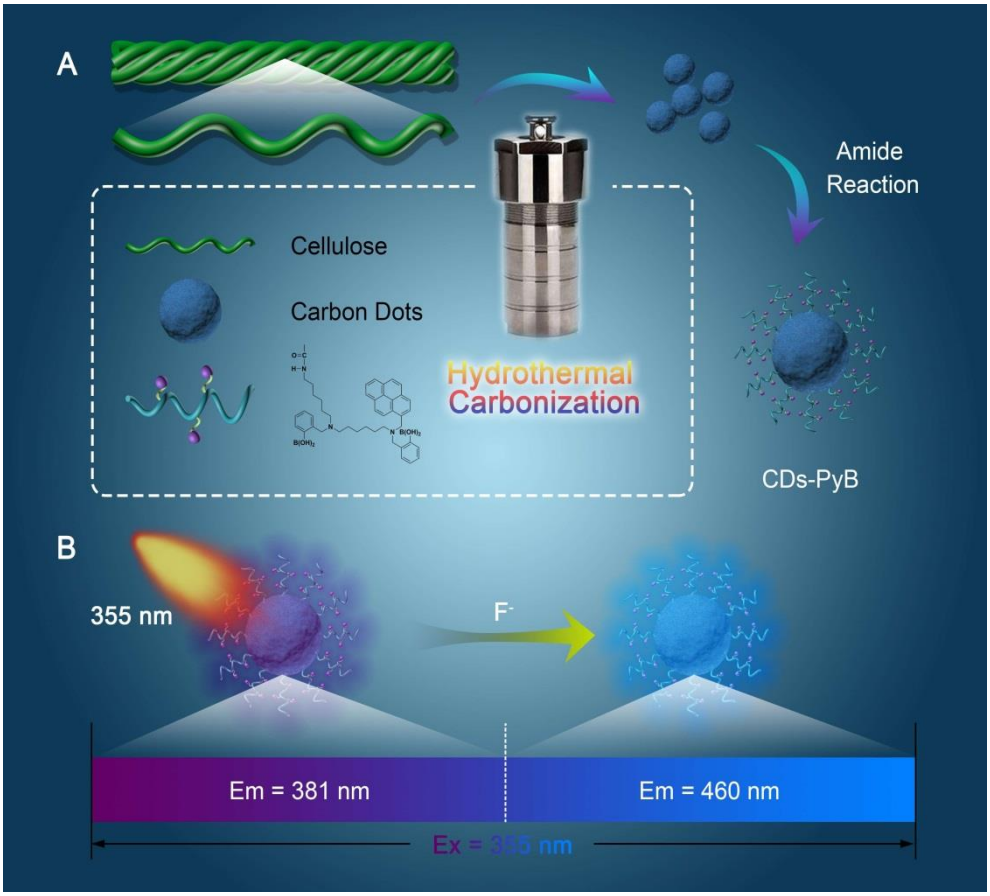

Scheme 1 Schematic illustration of the preparation of CDs-PyB and ratiometric detection of the CDs-PyB in response to F^-.

2. Methods

2.1 Materials

Carboxymethylated nanocellulose (C-CNC), ethylenediamine (EDA), N-(3-(dimethylamino)propyl)-N′-ethylcarbodiimide hydrochloride (EDC), N-hydroxysuccinimide (NHS) and trifluoroacetate were purchased from Sigma-Aldrich. Polyvinyl alcohol was obtained from Tianjin Kermel Reagent Co., Ltd. Sodium carboxymethyl cellulose was purchased from Sinopharm Chemical Reagent, CP. Ethanol absolute, and tetrahydrofuran (THF) were provided by Tianjin Kermel

Reagent Co., Ltd. Sodium fluoride, sodium chloride, sodium bromide, sodium sulfate and sodium dihydrogen phosphate were supplied by Tianjin Beichen Founder Reagent Factory. Dialysis membranes (1000 MWCO) were purchased from Green Bird Technology Development Co., Ltd. The water used in all experiments was deionized water. The chemical structures and molecular weights of all materials/reagents used are provided in Table S1.

2.2 Instruments

UV-Vis absorption spectra of the samples were performed using a T6 New Century ultraviolet-visible spectrophotometer. Fluorescence spectra were measured using a F97Pro fluorescence spectrophotometer. A Leici PXSJ-216F was employed to follow the F^- ion concentration in solution.

2.3 Synthesis of Carbon dots (CDs)

C-CNC (0.9 g) was dissolved in 60 mL deionized water for two hours using ultrasound to obtain a homogeneous solution. The solution was then transferred to a 100 mL autoclave and heated for 4 h at 240 ℃. After cooling to room temperature, the mixture was centrifuged at 8000 rpm for 8 min to obtain a yellow-brown supernatant. The obtained yellow-brown solution was filtered through a syringe and dialyzed in a dialysis bag for 48 h. Finally, the carbon dots were dried in a freeze dryer.

2.4 Synthesis of CDs-PyB composites

The pyrene-based boronic acid fluorescent probe PyB was synthesized as described in our previous paper [43]: bis(hexamethylene) triamine and $(Boc)_2O$ were reacted to

produce a mono-boctriamine derivative, and then the resulting amine was used in a reductive amination reaction with pyrene carboxyaldehyde. The intermediate was then reacted with pinacol protected 2-(bromomethyl)phenylboronic acid followed by deprotection to produce the desired probe molecule.

CDs (50 mg) were immersed in 80% THF solution, and then EDC (12.5 mg, 0.07 mmol) and NHS (18.75 mg, 0.16 mmol) were added to the solution under continuous stirring. The pH of the mixture was adjusted to 7-8 with NaOH and stirred for 30 min. 17.42 mg of PyB from above was added to the solution and stirred continuously for 24 h at room temperature. After the reaction was complete, the solution was dialyzed against deionized water using a dialysis bag (1000 D) for 6 h to remove unreacted reagents. The CDs-PyB composites were obtained under freeze drying.

2.5 Preparation of cellulose membrane

First, 0.8 g CMC and 0.8 g polyvinyl alcohol were dissolved in 50 mL of deionized water to prepare a homogeneous solution. Then, 920 mg EDC (4.8 mmol) and 664 mg NHS (5.7 mmol) were added into the CMC solution. The pH of the resulting mixture was adjusted to 7.5-8 by aqueous solutions of NaOH and HCl. After mixing for 30 min, EDA was added to the solution at room temperature and left for 24 h. Then, 50 mL polyvinyl alcohol solution and 1 mL CDs-PyB (100 μg/mL) were added and stirred for 30 min. The membranes were prepared by pouring the solution into polystyrene petri dishes then allowing them to dry at a temperature of 40 ℃ and a relative humidity (RH) of 50%. The obtained membrane was washed with ethanol solution three times.

2.6 Characterization

Transmission electron microscopy (TEM) was used to observe the structure of the samples using a JEM 2100 transmission electron microscope (JEOL Ltd., Tokyo, Japan) at an accelerating voltage of 200 kV. X-ray powder diffraction (XRD) patterns were measured using an X-ray diffractometer (Bruker, Germany) at a wide angle (10-80 °) scan in steps of 0.01 degrees. Fourier transform infrared (FT-IR) spectra spectrophotometer (Thermo Electron Nicolet-360, USA) were performed to explore the chemical structures on the surface of the samples. Scanning electron microscopy (SEM, JSM-7600F, JEOL, Japan) was used to explore the morphology of the membranes. The elements were analyzed by Thermo Scientific Ultra Dry SDD Energy-dispersive X-ray spectroscopy (EDS). The chemical composition of samples was examined using the X-ray photoelectron spectrum (XPS) on a Thermo Scientific: Escalab250Xi.

2.7 Fluorescence measurements

Fluorescence spectra of samples were obtained using a F97Pro Fluorescence Spectrophotometer. The excitation and emission slits were set to mid condition and the voltage to 220 V. 100 μg/mL of CDs-PyB was prepared in EtOH-H_2O (1:3, v/v). NaF, NaBr, NaCl, $NaSO_4$, NaH_2PO_4 solutions were prepared in aqueous solution. Different concentrations of NaF solution were gradually added to CDs-PyB solution in a quartz cuvette for measuring. Solutions of the other sodium salts were prepared under the same conditions.

2.8 Fluorescence detection by CPC membrane

The prepared membrane 2 cm ×1 cm was pasted onto a quartz slide. The slide was then placed into a cuvette containing 2 mL of solvent. The F^- solutions were then added gradually for investigating the fluorescence behavior.

2.9 Adsorption measurements

Solutions were prepared by dissolving NaF in deionized water. The F^- solution was filtered using a buchner funnel with diameter 40 mm. The F^- concentration was measured by a Leici PXSJ-216F fluoride ion meter (Shanghai).

The influence of various parameters such as initial concentration of the F^- and pH was then evaluated. The equilibrium adsorption capacity (Q_e) and the removal efficiency (E) were determined using these equations [44]:

$$Q_e = \frac{(C_0 - C_e)}{m} V \quad (1)$$

$$E = \frac{C_0 - C_e}{C_0} \times 100\% \quad (2)$$

Where C_0 and C_e are initial and equilibrium concentrations (mg L^{-1}) of the F^- solution, respectively. V (L) is the volume of solution and m (g) is the weight of the membrane.

2.10 Recyclability

The recyclability of the CPC membrane was measured using 5 mg L^{-1} F^- at 25 ℃. The regeneration of the membrane was carried out by washing these membranes with 100 mL of 1.0 mol L^{-1} HNO_3 solution and aqueous solution. The regenerated membranes were used for further filtration of fluoride.

2.11 Cell proliferation assay

HT 29 cells were used as model cells in the following experiments. Cells were

cultured in 96-well plates at a density of 1×10^4 cells per well. The cells were maintained in Eagle's minimum essential medium (MEM) with 10% fetal bovine serum at 37 ℃ and 5% CO_2 in a humidified incubator. Then, the medium containing the membranes (3 × 3 mm) was added and incubated for 1, 3 and 5 days. The cells were washed twice with PBS to remove the culture medium. 200 μL fresh culture medium and 30 μL of 3-(4,5-dimethylthiazol-2-yl)-2,5-diphenyltetrazolium bromide (MTT) solution (5 mg mL^{-1} in PBS) were added to each well and incubated for another 4 h at 37 ℃. Finally, the absorbance was collected at 570 nm with the 96-well plate reader Tecan Infinite F200 PRO, and the cell viability values were calculated. The cell viability is obtained by the following formula:

cell viability (%) = [(the absorbance of samples- the absorbance of blank)/(the absorbance of control group- the absorbance of blank)] × 100%.

2.12 Live/dead viability assay

The live/dead viability of membranes was evaluated on HT 29 cell lines. Cells were seeded at a density of around 5×10^3 per mL to a glass dish and cultivated for 24 h. The assay for 1, 3, and 5 days was further applied on membranes (10 × 10 mm) to evaluate the live/dead viability. Cells were then washed twice with PBS and stained according to the kit instructions (Gibco, Life Technologies, USA). The cells were stained with 500 μL Live/Dead viability/cytotoxicity kit for 15 min at room temperature in the dark, and the cells imaged under a confocal microscope (Leica TCS SP8). The live and dead cells were labeled with green (calcein AM, 2 μM) and

red (EthD-1, 4 μM).

3. Results and discussion

3.1 The fluorescence properties of PyB

The boronic acid based fluorescent probe was prepared as described previously [43]. The emission spectra of the PyB were investigated to understand its F^- recognition behavior. Upon the addition of F^- ions, the fluorescence of the PyB at 382, 396, 421 nm was significantly enhanced (Fig. S1), confirming that the PyB could be used as an attractive approach for the detection of F^- ions. However, the PyB molecule suffers from poor solubility, which could compromise the sensing efficiency in an aqueous system. In order to improve the solubility and sensitivity for the detection of F^-, we introduced carbon dots (CDs) as an energy acceptor on which to attach the PyB molecule and to fabricate a FRET system [45].

3.2 The characterization of CDs and CDs-PyB

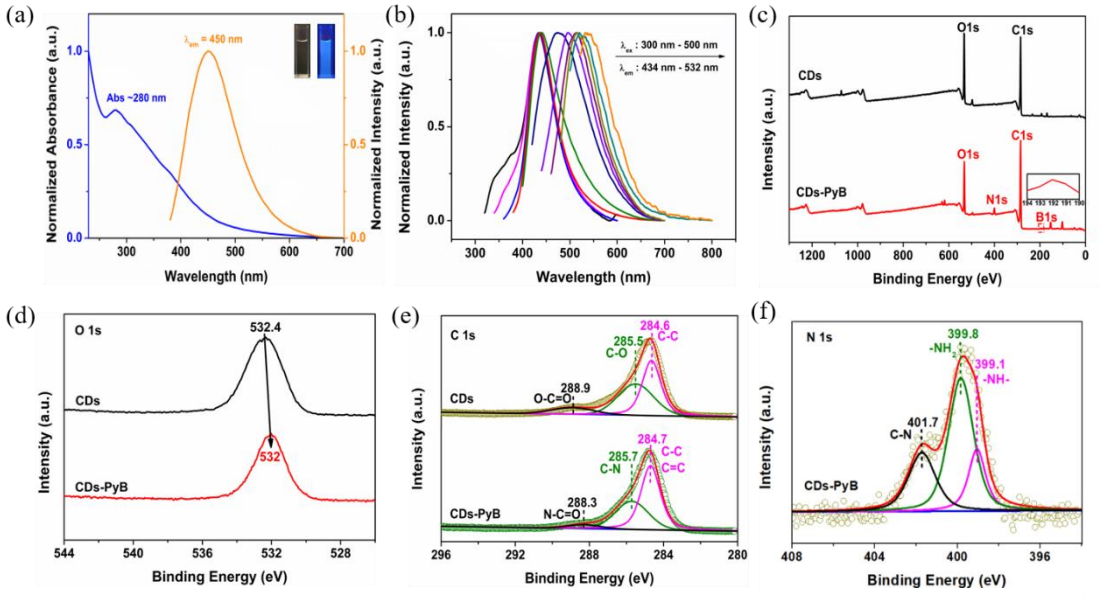

Fig. 1 (a) Absorbance and emission spectrum of CDs in aqueous solution (100 μg mL^{-1}). Insert: photographs of CDs in water under white light and 365 nm UV light (right); (b)

Normalized fluorescent emission spectra of the CDs (100 μg mL^{-1}) aqueous solution at different excitation wavelengths; XPS spectra of CDs and CDs-PyB: (c) survey spectra of CDs and CDs-PyB; (d) O 1s and (e) C 1s of CDs and CDs-PyB; (f) N 1s of CDs-PyB.

X-ray diffraction (XRD) analysis of the CDs was then performed. The XRD pattern in Fig. S2 displayed a broad band at 23.1 °, which confirmed that the composition of CDs is highly disordered carbon atoms [46]. The morphology of the synthesized fluorescent CDs was observed via TEM. TEM images revealed that the CDs were monodisperse and had a spherical morphology (Fig. S3) [47]. UV-vis absorption and emission spectra of the CDs were then investigated in aqueous solution (Fig. 1a). An absorption band was observed at around 280 nm and a peak centered at 450 nm was observed in the emission spectrum when excited at 360 nm. As shown in Fig. 1b, the excitation-dependent photoluminescence behavior of the CDs was observed, which is typical of the optical emission of CDs. With excitation wavelengths in the range 300-500 nm, fluorescence emission was observed over the range 434-532 nm. Therefore, the as prepared CDs could be employed to match a specific energy donor with a suitable excitation wavelength. The emission band position varied according to excitation wavelength used, which may be ascribed to the different emissive sites on the CDs [45, 48, 49]. Additionally, the CDs solution displayed the most intense intensity at around 450 nm with excitation at 360 nm, and the emission band was gradually red-shifted when the excitation wavelength was varied.

The Fourier Transform Infra-Red (FTIR) of CDs, PyB and CDs-PyB are shown in Fig. S4, in which the typical characteristic peaks at 1309 cm^{-1} and 1600 cm^{-1} can be ascribed to the C-N and N-H stretching vibrations of CDs-PyB, indicating the pyrene

was successfully attached to the CDs. The X-ray photoelectron spectroscopy (XPS) was obtained to identify the chemical composition of the CDs and CDs-PyB, as shown in Fig. 1. XPS revealed that the CDs mainly consisted of C and O elements, indicative of the presence of hydroxyl and carboxylic acid groups on the surface (Fig. 1c). Additionally, the full survey of CDs-PyB clearly shows an apparent peak at 407.48 eV, corresponding to the signals from the N-H group. The peak of B 1s at 192.1 eV in the XPS spectrum demonstrates the B element in the CDs-PyB [50]. For the O 1s spectra, the peak at 532.4 eV on CDs is considered to be the C=O bond of carboxyl group, while the peak appears slightly shifted at 532.0 eV for the CDs-PyB (Fig. 1d) [51]. The shift demonstrates the changed in environment of the O atoms in CDs-PyB, which can be ascribed to the amide bond formation between the CDs and the PyB. The XPS C 1s spectra of the CDs and CDs-PyB are displayed in Fig. 1e. The spectrum of C 1s in CDs could be approximately split into three peaks at 284.6eV, 285.5eV and 288.9 eV, which were ascribed to the C-C, C-O and O-C=O [51, 52]. The C-O and O-C=O peaks can be attributed to hydroxyl and carboxyl groups of the CDs. While in the sample of CDs-PyB, a slight change at 284.7eV, 285.7eV and 288.3 eV was observed, which may be assigned to the C-C/C=C, C-N and N-C=O bond [16, 53]. Fig. 1f shows the spectra for the N 1s core level, the peak can be mainly divided into three typical peaks located at about 399.1 eV, 399.8 eV and 401.7 eV, which could be considered to be -NH-, -NH_2 and C-N, respectively [53-55]. These results further confirm the bonding between the CDs and PyB.

3.3 Sensing of F^- with CDs-PyB

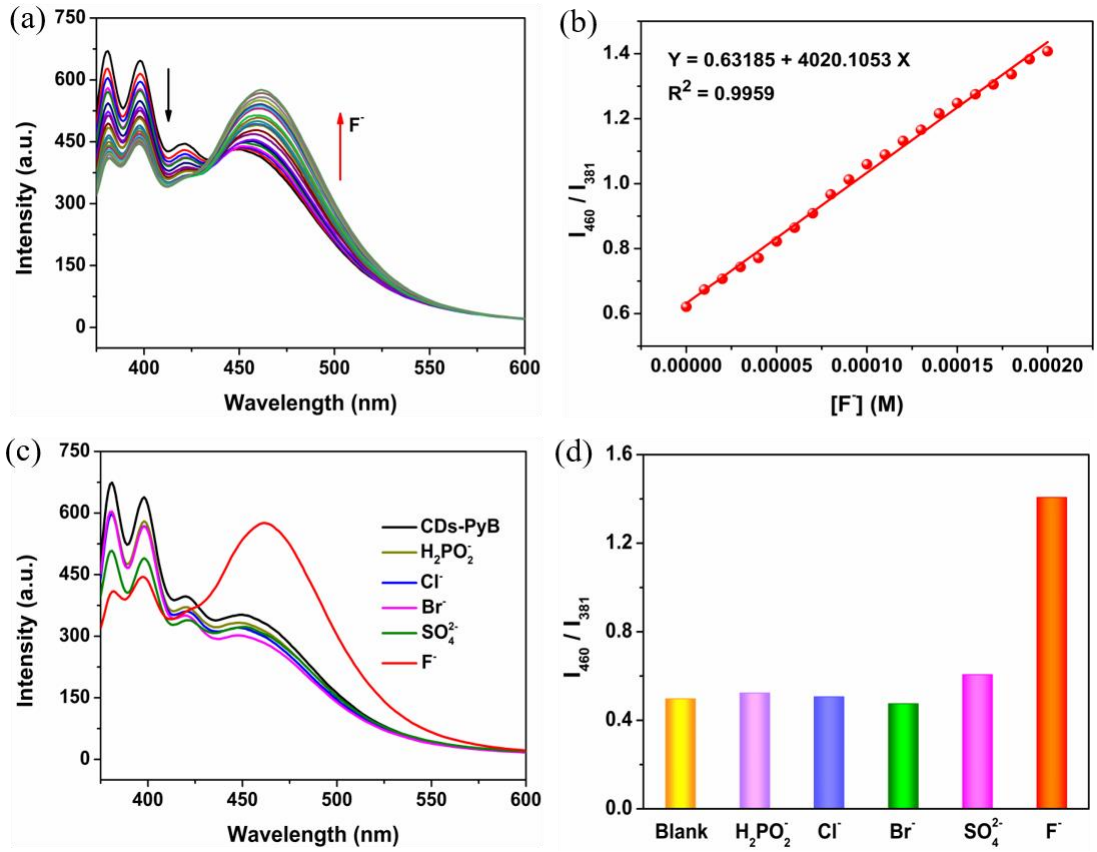

Fig. 2 (a) Fluorescence emission spectra of the CDs-PyB (25 μg mL^{-1}) with the addition of different concentrations of F^- (0-200 μM) (λ_{ex}= 355 nm); (b) Fluorescence intensity ratios (I_{460}/I_{381}) of the CDs-PyB (25 μg mL^{-1}) in the presence of different amounts of F^- (λ_{ex}= 355 nm); (c) Fluorescence emission spectra and (d) ratios (I_{460}/I_{381}) of CDs-PyB (25 μg mL^{-1}) upon addition of various anions (1×10^{-2} M) (λ_{ex}= 355 nm).

Having determined the chemical structure of the CDs-PyB, we next investigated their fluorescence properties. UV-vis absorption spectra of CDs-PyB were measured (Fig. S5). A slight decrease in UV absorbance was observed upon addition of F^- ions. To investigate the detection behavior of F^-, CDs-PyB was treated with various amounts of F^-. As shown in Fig. 2a, there was a significant reduction in the emission intensity at 381 nm with concomitant enhancement in the emission at 460 nm with the addition of F^- to the CDs-PyB solution. Moreover, it was found that the emission intensity of CDs at about 460 nm was nearly unchanged with addition of F^- (Fig. S6). These results

further demonstrate that the introduction of F^- could induce dual changes in the emission, suggesting that the ratiometric detection of F^- was possible. To investigate the sensing mechanism, the optical properties of PyB and CDs were investigated. Initially, PyB showed emission at the wavelength of 381 nm upon the excitation of 355 nm, which can be absorbed by the CDs (Fig.1a and S1). We propose that this causes dual emission of the CDs-PyB (381 nm and 460 nm) upon 355 nm excitation. The addition of F^- triggers the fluorescence enhancement of the pyrene moiety (Fig. S1). Meanwhile, the distance between CDs and the pyrene may be reduced due to the interaction the charged boronate (F^- bound to the boronic acid) and strongly hydrogen bonding amide groups [56], facilitating energy transfer between PyB and the CDs. Which, results in enhancement of the fluorescence signal at 460 nm and reduction of the fluorescence at 381 nm. Such ratiometric sensors with different wavelengths can accomplish highly sensitive and accurate detection of anions using internal calibration of the two emission signals [57-59]. In the concentration range of 0 to 200 μM, the fluorescence intensity ratio of the CDs-PyB nanosensor is linearly proportional to the concentration of F^-, as shown in Fig. 2b. The calculated R^2 of 0.996, indicates excellent linear ratiometric fluorescence response towards F^-. The detection limit of the CDs-PyB nanosensor for F^- was determined from the emission ratio of the two wavelengths (I_{460}/I_{381}) and calculated to be 5.9×10^{-5} M (LOD = 3σ/k, where σ is the standard deviation of the blank measurements, and k is the slope of the intensity vs sample concentration), which was comparable to previous reports indicating that the nanosensor exhibited high

sensitivity for F^- [60-62]. Additionally, the fluorescence response of the CDs-PyB to different anions was evaluated. As shown in Fig. 2c, it was found that only the addition of F^- ions enhances the intensity of the fluorescence, while other anions display only subtle changes of the CDs-PyB spectra at 460 nm. In addition, the intensity ratio (I_{460}/I_{381}) of the CDs-PyB nanosensor in the presence of other anions is nearly unchanged. With the addition of F^- ions, there was a significant ratiometric change in the fluorescence emission intensity (Fig. 2d). These results demonstrate the selectivity of the CDs-PyB nanosensor towards F^- over the other anions. Therefore, for CDs-PyB, the ratiometric sensing is a highly-sensitive and selective method to detect F^- ions.

3.4 Fluorescence sensing and adsorption studies for F^- with CPC membrane

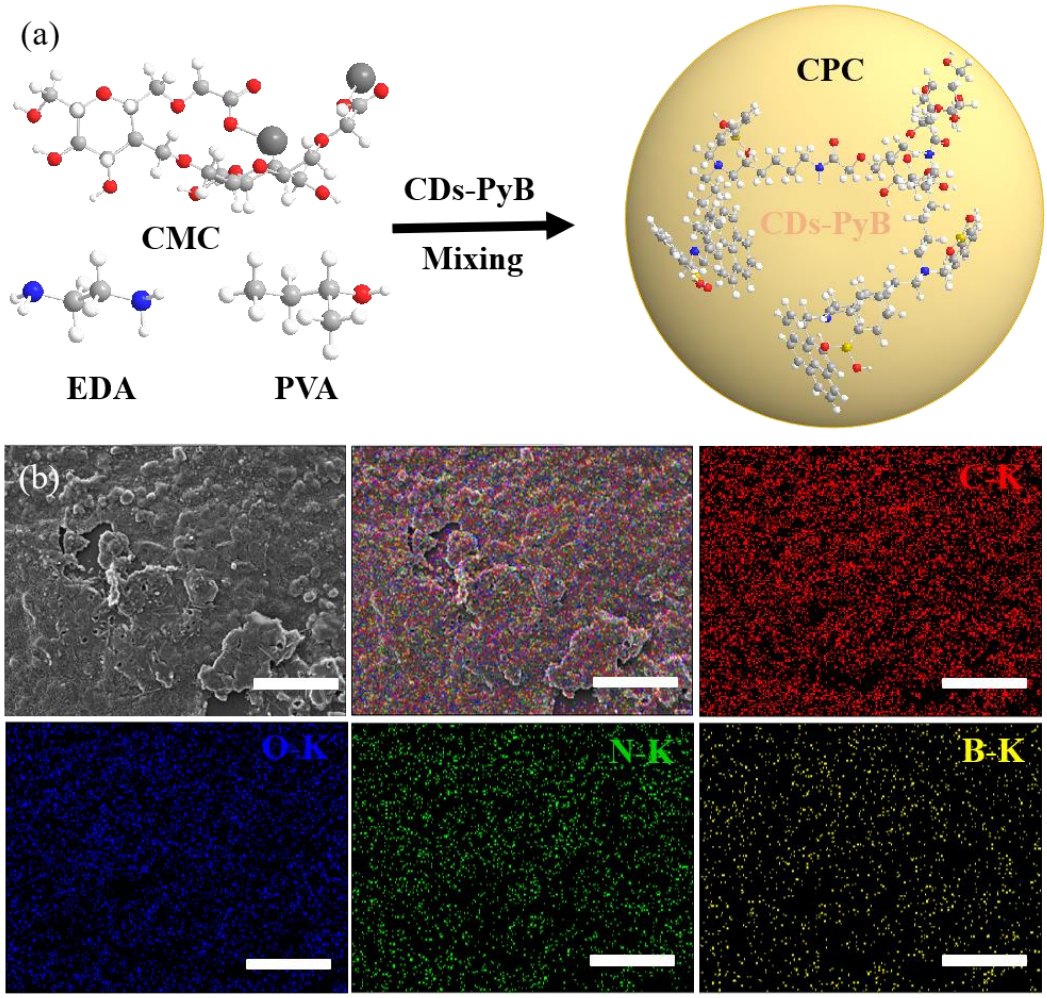

Fig. 3 (a) Schematic Illustration of the preparation of an CPC membrane; (b) SEM image of the CPC membrane and EDS-mapping areas of the CPC membrane (scale bar = 100 μm).

Encouraged by the detection performance of the CDs-PyB, we proceeded to investigate the detection and removal potential of amino-modified cellulose membrane containing CDs-PyB (CPC membrane) (Fig. 3a). The amino-modified cellulose (AMC) membrane was first investigated, since the amine functional groups could enhance the removal of F^-. FTIR spectroscopy was employed to understand the structure of the amino-modified cellulose membrane. The peak at 1635 cm^{-1} was attributed to the carbonyl group of the amide, while the peak at 3286 cm^{-1} was assigned to the N-H groups (Fig. S7), indicating the successful amide modification [63, 64]. The CPC

membrane was prepared by the mixing of the CDs-PyB with amino-modified cellulose through self-assembly via hydrogen bonding between the hydroxyl groups of the CDs and cellulose chain. The CDs could be used as an intermediate to reduce the aggregation of the PyB moiety, which facilitates the detection ability of the membrane. As shown in Fig. 3b, SEM was performed to confirm the dense structure of the CPC membranes. Moreover, the EDS images demonstrated that the C, O, N, and B elements were dispersed on the surface of CPC membranes, suggesting the CDs-PyB were associated with the membrane successfully.

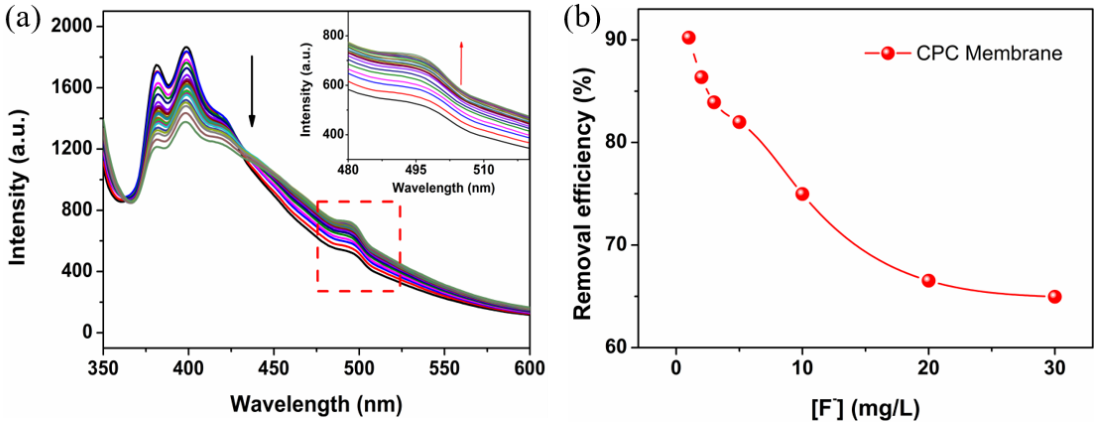

Fig. 4 Fluorescence emission spectra of the CPC membrane in ethanol solution with the addition of different concentrations of F^- (0-200 μM) (λ_{ex}= 330 nm); (b) anion uptake of the CPC membrane as a function of F^- ion concentration.

The application of the synthesized CPC membrane for F^- recognition was subsequently explored. The CPC membrane may retain some sodium chloride. However, according to related literature, the ionic strength due to the co-existence of Na^+ and Cl^- has little effect on the fluorescence response [65]. To further investigate the fluorescence sensing behavior for F^-, the CPC membrane in the presence of different amounts of F^- was measured. In the absence of F^-, the CPC membrane displays almost

no emission when excited at 330 nm and no time dependent change was observed, demonstrating that the CPC membrane is quite stable. With addition of F^-, the fluorescence of the CPC membrane at 380-420 nm was significantly reduced, whereas at 495 nm the intensity was increased (Fig. 4a). This phenomenon may be ascribed to the appearance of energy transfer from the pyrene to the CDs. In addition, the relationship between the intensity ratios (I_{495}/I_{381}) and the concentration of F^- was measured (Fig. S8). The fluorescence intensity ratio demonstrated a good linear correlation ($R^2 = 0.954$) with the concentrations of F^- over a range from 0-200 μM [66]. These results indicated that the CPC membrane could be exploited as a sensor for the detection of F^-. Subsequently, the removal ability of the CPC membrane was investigated. Firstly, the initial concentration-dependent removal of F^- on the prepared membranes was measured. It was found that the F^- uptake capacity of the CPC membrane was in the range of 90.2-64.9% with increasing F^- concentration from 1 to 30 ppm (Fig. 4b). The data suggests that the CPC membrane can effectively extract F^- at low concentrations from wastewater. In addition, the CPC membrane displays reasonable retention performance for high concentrations of F^-. These results may be ascribed to the electrostatic interaction between F^- and the amino groups of the membrane [67]. The pH of wastewater is an important factor in membrane treatment. Hence, we investigated the pH on the retention capacity of F^- over a pH range from 1.0-11.0. It can be seen that there is no significant change in the retention capacity from pH 1.0 to 11.0. However, the best filtration occurs under neutral pH conditions

(Fig. S9a). This result suggests that the membrane is not affected by pH, making it suitable for a wide range of industrial applications for various wastewaters under a harsh environment. The recyclability of the CPC membrane is important in pollution control and environmental protection. As shown in Fig. S9b, after three desorption cycles, the recyclable adsorption behavior of the CPC membrane towards F^- was almost unchanged with the retention capacity of the CPC membrane only decreasing slightly. The removal efficiency of the CPC membrane for F^- after one and three cycles was 82.7% and 73.9%, respectively. The excellent uptake capacity reveals that the CPC membrane could be an effective adsorbent for environmental remediation.

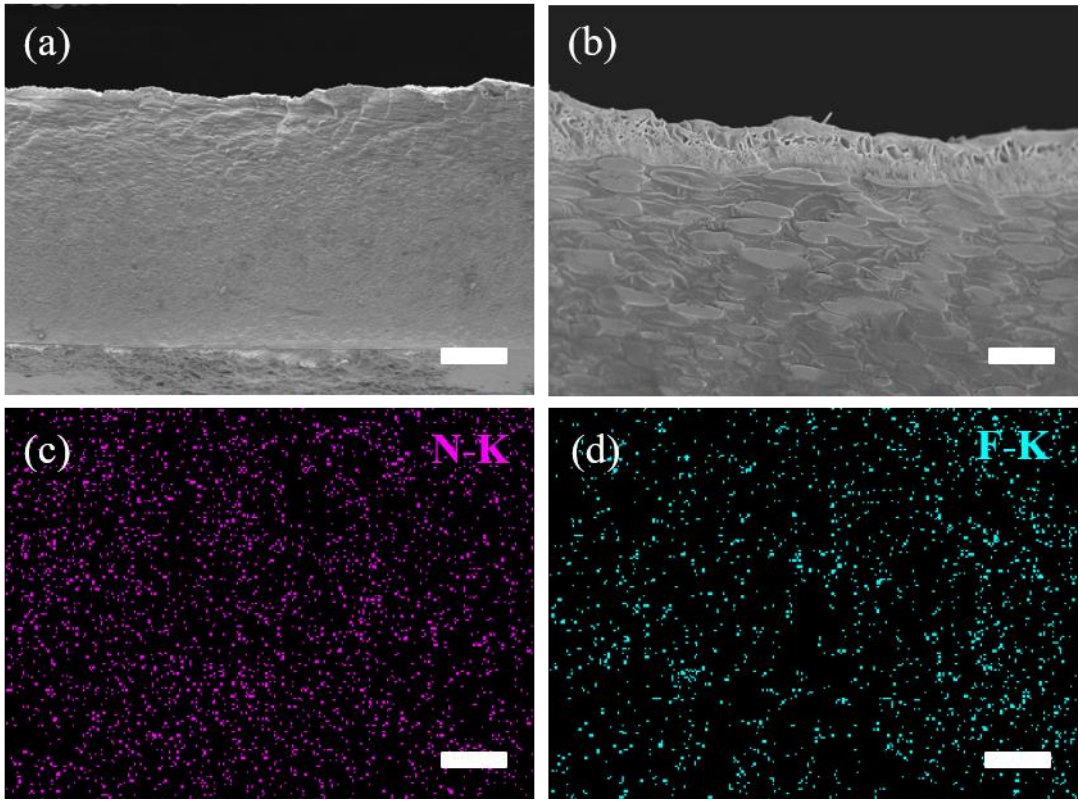

Fig. 5 (a) Cross-sectional SEM images of the CPC membrane and (b) in magnified mode; and EDS mapped areas of the CPC membrane after F^- filtration containing (c) N and (d) F.

The fluoride removal mechanism by CPC membrane may be ascribed to the

electrostatic interaction between F^- and the membrane [67, 68]. The $-NH_2$ of the membrane can be protonated in aqueous solutions to form $-NH_3^+$. The protonated amino groups ($-NH_3^+$) can adsorb negatively charged fluoride ions through hydrogen bonding and ionic interactions [69]. To further verify the retention capacity of the F^- in the membrane and understand the retention mechanism, cryogenic scanning electron microscopy (cryo-SEM) together with energy dispersive X-ray spectroscopy (EDS) was conducted. As shown in Fig. 5a and 5b, the cross-section SEM images display a porous scattering of cellulose layers in the CPC membrane, which could provide more binding sites for the F^-. From the EDS mapping (Fig. 5c), it can be seen that the N are uniformly distributed within the CPC membrane layer, which can contribute to the retention efficiency of the F^-. It is also found that the fluoride ions are evenly distributed within the CPC membrane layer after the removal process (Fig. 5d). The uniformly dispersed F^- in the membrane indicates that the extraction of F^- is through absorption. Moreover, the success of the CPC membrane synthesis was confirmed by the presence of N in the EDX (Fig. S10a). In Fig. S10b, the EDX results verified the presence of F^- ions after filtration, suggesting F^- ions were adsorbed by the membrane layer successfully. These results indicate that the surface modification and the pore structure of the membrane have a positive effect on the F^- removal. This research not only deepens the understanding of F^- adsorption behavior but also provides a promising and highly efficient adsorbent for removing F^- ions from industrial wastewater. This system also confirms that the membrane can synergistically detect and adsorb fluoride

ions. Thus, the dual-function sensor system could provide a promising practical membrane for monitoring and removal of hazardous pollutants.

3.5 Cytocompatibility assay of membrane

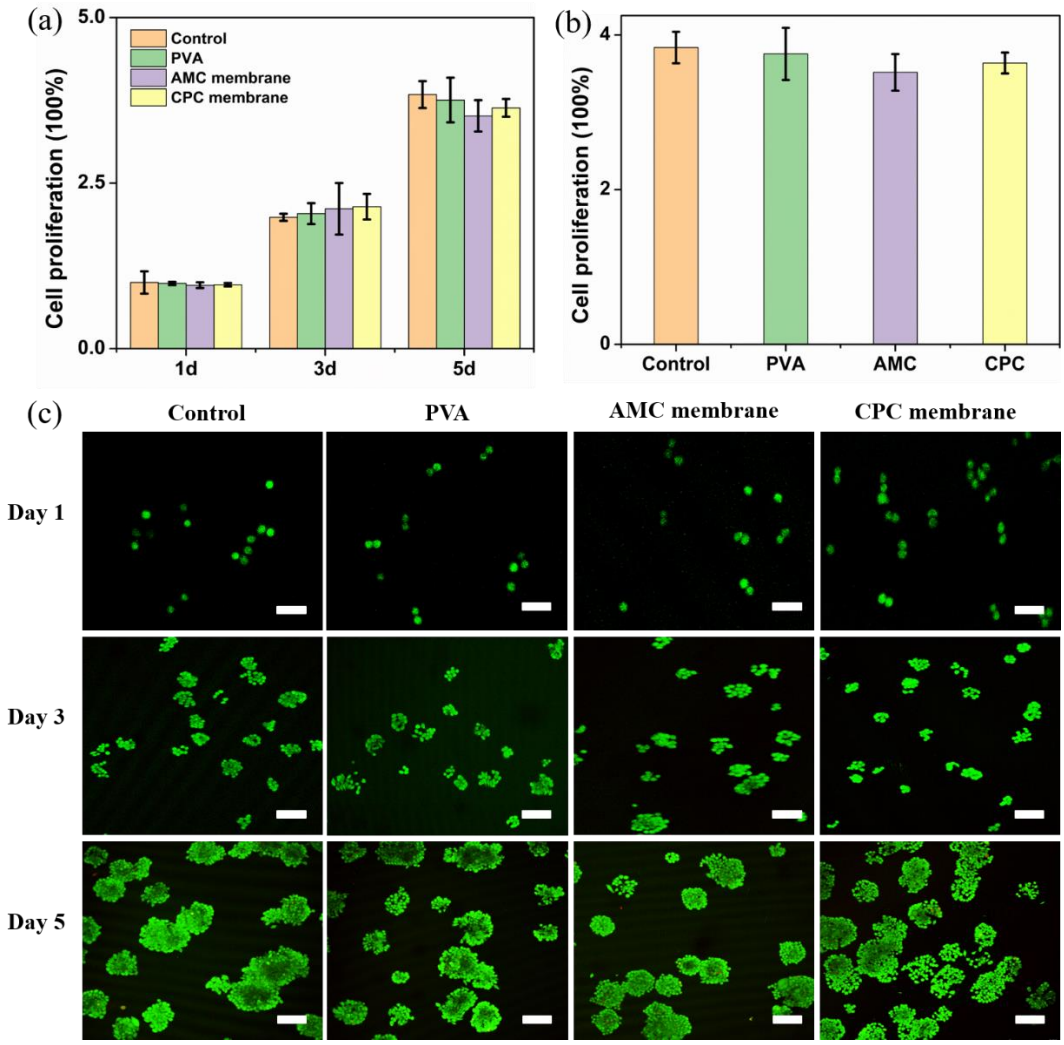

Fig. 6 (a) Cell proliferation assay of the control, PVA, AMC membrane and CPC membrane after cell cultures of 1, 3, and 5 days, respectively; (b) Cell proliferation assay of the control, PVA, AMC and CPC membrane after cell cultures of 5 days; (c) Representative fluorescent images of live/dead assay for different membranes after cultures of 1, 3, and 5 days, respectively.

The desirable fluorescence properties of the membrane for F^- prompted us to exploit its cytocompatibility. The cell viability of the CPC, AMC, PVA membrane and control were examined by in vitro culture of HT 29 cells. The cell proliferation of the

membranes was determined through MTT assay using HT 29 cells. Cells were respectively assessed after 1, 3 and 5 days of culture on membranes (Fig. 6a). The results demonstrated that the cell viability remained and similar cell density was observed when the cells were cultured for 1 day. Moreover, the cell viability values increased as the cells were cultivated for 3 days, and even increased almost 4 times after 5 days (Fig. 6b), which suggests that all the membranes are not cytotoxic. In addition, no negative effects on the fluorescence were observed during the test period. Confocal fluorescence images of HT 29 cells cultured with membranes are shown in Fig. 6c. Compared to the control, the cells on the membranes displayed a similar cell density after the first day's culture. However, after culturing for 5 days, it can be seen that the cells almost entirely covered the membranes and the control, confirming the non-toxicity of the samples. Furthermore, similar live cell (green) density without noticeable dead cells (red) were observed for all the three samples after culturing for 1 day and even during prolonged culture, only a few dead cells were observed, which was in accordance with the MTT results. These results indicate that the CPC membrane has no negative effects on cell quantity or morphology and HT 29 cells hold their typical oblong shape during the whole incubation period. Based on the excellent biocompatibility, these membranes would be suitable for potential biomedical and environmental applications.

3.6 Cost efficiency of the CPC membrane

Moreover, we have performed a cost comparison to verify the cost efficiency of the

CPC membrane for further practical environmental applications. As shown in Tables S2-S5, it can be seen that the CPC membrane costs about 0.117 dollars per gram compared to the common polymer membranes for detection and removal of pollutants. In contrast, the cost of the polymer membrane is about 3.518 and 3.081 dollars for 1 g and 0.819 dollars for graphene membranes, respectively [70-72]. These results indicate that the CPC membrane could provide a cost-effective strategy for the detection and removal of contaminants from waste water.

4. Conclusion

In summary, we have successfully developed a novel ratiometric nanosensor using a pyrene-boronic acid based fluorescent molecule and carbon dots as the energy donor-acceptor pair for selectivity detecting F^-. The as-prepared nanosensor displayed a sensitive, linear dependence, and rapid response to F^-. Upon addition of F^-, the fluorescence intensity ratio of the CDs to PyB (I_{460}/I_{381}) was linearly proportional to the concentration of F^- ions over a wide range from 0 to 200 μM. The CDs-PyB also displayed excellent selectivity for F^-. Furthermore, the amino-modified cellulose membrane-based sensor containing the CDs-PyB displayed rapid sensing and excellent extraction capacity for F^-. The MTT assay verified that the CPC membrane has excellent biocompatibility. Such cellulose-based sensors could provide a dual-functionality for both sensing and removal of F^- with the potential advantages of processability, cost effectiveness and environmental friendliness. We anticipate that this approach could provide a strategy for designing and investigating diverse

functional membranes for the detection and adsorption of other pollutants by just swapping the selective fluorescent probe. For future industrial applications, the economic efficiency and comprehensiveness of the adsorbent are crucial factors. Therefore, future research should focus on investigating multifunctional and economical adsorbents and studying the potential of cellulose-based sensors for industrial wastewater in a continuous flow fixed-bed column.

Abbreviations

A table containing the abbreviations used in the manuscript has been included in the ESI (Table S6).

Notes

The authors declare no conflicts of interest.

Acknowledgements

The present work is supported by the National Natural Science Foundation of China (Grant #: 21607044, 31800494). This work was also supported by Natural Science Foundation of Hebei Province (Grant #: B2017502069) and the Fundamental Research Funds for the Central Universities (Grant #: 2018MS113), the Young Elite Scientists Sponsorship Program by CAST (2018QNRC001). TDJ wishes to thank the Royal Society for a Wolfson Research Merit Award.

References

[1] S. Dong, Y. Wang, Characterization and adsorption properties of a lanthanum-loaded magnetic cationic hydrogel composite for fluoride removal, Water

Res. 88 (2016) 852-860.

[2] G. Nie, Y. Sun, F. Zhang, M. Song, D. Tian, L. Jiang, H. Li, Fluoride responsive single nanochannel: click fabrication and highly selective sensing in aqueous solution, Chem. Sci. 6 (2015) 5859-5865.

[3] S. Zhang, J. Fan, S. Zhang, J. Wang, X. Wang, J. Du, X. Peng, Lighting up fluoride ions in cellular mitochondria using a highly selective and sensitive fluorescent probe, Chem. Commun. 50 (2014) 14021-14024.

[4] T. Poursaberi, M. Hassanisadi, K. Torkestani, M. Zare, Development of zirconium (IV)-metalloporphyrin grafted Fe_3O_4 nanoparticles for efficient fluoride removal, Chem. Eng. J. 189-190 (2012) 117-125.

[5] X. Chen, S. Yu, L. Yang, J. Wang, C. Jiang, Fluorescence and visual detection of fluoride ions using a photoluminescent graphene oxide paper sensor, Nanoscale 8 (2016) 13669-13677.

[6] K.M.K. Swamy, Y.J. Lee, H.N. Lee, J. Chun, Y. Kim, S.-J. Kim, J. Yoon, A new fluorescein derivative bearing a boronic acid group as a fluorescent chemosensor for fluoride ion, J. Org. Chem. 71 (2006) 8626-8628.

[7] M. Li, Z. Liu, H.C. Wang, A.C. Sedgwick, J.E. Gardiner, S.D. Bull, H.N. Xiao, T.D. James, Dual-function cellulose composites for fluorescence detection and removal of fluoride, Dyes Pigments 149 (2018) 669-675.

[8] X. Zhang, L. Guo, F.-Y. Wu, Y.-B. Jiang, Development of fluorescent sensing of anions under excited-state intermolecular proton transfer signaling mechanism, Org.

Lett. 5 (2003) 2667-2670.

[9] C. Duan, M. Won, P. Verwilst, J. Xu, H.S. Kim, L. Zeng, J.S. Kim, In vivo imaging of endogenously produced HClO in zebrafish and mice using a bright, photostable ratiometric fluorescent probe, Anal. Chem. 91 (2019) 4172-4178.

[10] Q. Zhao, C. Zhang, S. Liu, Y. Liu, K.Y. Zhang, X. Zhou, J. Jiang, W. Xu, T. Yang, W. Huang, Dual-emissive polymer dots for rapid detection of fluoride in pure water and biological systems with improved reliability and accuracy, Sci. Rep. 5 (2015) 16420.

[11] P. Ashokkumar, H. Weisshoff, W. Kraus, K. Rurack, Test-strip-based fluorometric detection of fluoride in aqueous media with a BODIPY-linked hydrogen-bonding receptor, Angew. Chem. Int. Ed. 53 (2014) 2225-2229.

[12] W. Tian, J. Zhang, J. Yu, J. Wu, H. Nawaz, J. Zhang, J. He, F. Wang, Cellulose-based solid fluorescent materials, Adv. Optical Mater. 4 (2016) 2044-2050.

[13] Q. Hu, Q. Huang, K. Liang, Y. Wang, Y. Mao, Q. Yin, H. Wang, An AIE+TICT activated colorimetric and ratiometric fluorescent sensor for portable, rapid, and selective detection of phosgene, Dyes Pigments 176 (2020) 108229.

[14] M. Li, X. An, M. Jiang, S. Li, S. Liu, Z. Chen, H. Xiao, “Cellulose Spacer” strategy: anti-aggregation-caused quenching membrane for mercury ion detection and removal, ACS Sustainable Chem. Eng. 7 (2019) 15182-15189.

[15] R. Jia, W. Tian, H. Bai, J. Zhang, S. Wang, J. Zhang, Amine-responsive cellulose-based ratiometric fluorescent materials for real-time and visual detection of

shrimp and crab freshness, Nat. Commun. 10 (2019) 795.

[16] S. Chen, Y. Jia, G.Y. Zou, Y.L. Yu, J.H. Wang, A ratiometric fluorescent nanoprobe based on naphthalimide derivative-functionalized carbon dots for imaging lysosomal formaldehyde in HeLa cells, Nanoscale 11 (2019) 6377-6383.

[17] B. Ma, S. Wu, F. Zeng, Y. Luo, J. Zhao, Z. Tong, Nanosized diblock copolymer micelles as a scaffold for constructing a ratiometric fluorescent sensor for metal ion detection in aqueous media, Nanotechnology 21 (2010) 195501.

[18] L. Xian, H. Ge, F. Xu, N. Xu, J. Fan, K. Shao, X. Peng, Intracellular MicroRNA imaging using telomerase-catalyzed FRET ratioflares with signal amplification, Chem. Sci. 10 (2019) 7111-7118.

[19] H. Mehdi, W. Gong, H. Guo, M. Watkinson, H. Ma, A. Wajahat, G. Ning, Aggregation-induced emission (AIE) fluorophore exhibits a highly ratiometric fluorescent response to Zn^{2+} in vitro and in human liver cancer cells, Chem. Eur. J. 23 (2017) 13067.

[20] P. Anzenbacher, Jr., Y. Liu, M.A. Palacios, T. Minami, Z. Wang, R. Nishiyabu, Leveraging material properties in fluorescence anion sensor arrays: a general approach, Chem. Eur. J. 19 (2013) 8497-8506.

[21] J. Fan, H. Mu, H. Zhu, J. Du, N. Jiang, J. Wang, X. Peng, Recognition of HClO in live cells with separate signals using a ratiometric fluorescent sensor with fast response, Ind. Eng. Chem. Res. 54 (2015) 8842-8846.

[22] Y. Mei, P. Bentley, A ratiometric fluorescent sensor for Zn^{2+} based on internal

charge transfer (ICT), Bioorg. Med. Chem. Lett. 16 (2006) 3131-3134.

[23] A. Bianchi-Smiraglia, M.S. Rana, C.E. Foley, L.M. Paul, B.C. Lipchick, S. Moparthy, K. Moparthy, E.E. Fink, A. Bagati, E. Hurley, H.C. Affronti, A.V. Bakin, E.S. Kandel, D.J. Smiraglia, M.L. Feltri, R. Sousa, M.A. Nikiforov, Internally ratiometric fluorescent sensors for evaluation of intracellular GTP levels and distribution, Nat. Methods. 14 (2017) 1003-1009.

[24] C. Hou, Y. Xiong, N. Fu, C.C. Jacquot, T.C. Squier, H. Cao, Turn-on ratiometric fluorescent sensor for Pb^{2+} detection, Tetrahedron Lett. 52 (2011) 2692-2696.

[25] W. Zhang, R. Wang, W. Liu, X. Wang, P. Li, W. Zhang, H. Wang, B. Tang, Te-containing carbon dots for fluorescence imaging of superoxide anion in mice during acute strenuous exercise or emotional changes, Chem. Sci. 9 (2018) 721-727.

[26] W.-J. Wang, J.-M. Xia, X. Hai, M.-L. Chen, J.-H. Wang, A hybrid of carbon dots with 4-chloro-7-nitro-2,1,3-benzoxadiazole for selective detection of p-phenylenediamine, Environ. Sci.: Nano. 4 (2017) 1037-1044.

[27] F. Liu, W. Zhang, W. Chen, J. Wang, Q. Yang, W. Zhu, J. Wang, One-pot synthesis of $NiFe_2O_4$ integrated with EDTA-derived carbon dots for enhanced removal of tetracycline, Chem. Eng. J. 310 (2017) 187-196.

[28] Z. Huang, F. Lin, M. Hu, C. Li, T. Xu, C. Chen, X. Guo, Carbon dots with tunable emission, controllable size and their application for sensing hypochlorous acid, J. Lumin. 151 (2014) 100-105.

[29] S. Zhao, Y. Huang, R. Liu, M. Shi, Y.M. Liu, A nonenzymatic chemiluminescent

reaction enabling chemiluminescence resonance energy transfer to quantum dots, Chem. Eur. J. 16 (2010) 6142-6145.

[30] A. Chatzimarkou, T.G. Chatzimitakos, A. Kasouni, L. Sygellou, A. Avgeropoulos, C.D. Stalikas, Selective FRET-based sensing of 4-nitrophenol and cell imaging capitalizing on the fluorescent properties of carbon nanodots from apple seeds, Sensor. Actuat, B-Chem 258 (2018) 1152-1160.

[31] M. Deng, S. Wang, C. Liang, H. Shang, S. Jiang, A FRET fluorescent nanosensor based on carbon dots for ratiometric detection of Fe^{3+} in aqueous solution, RSC Adv. 6 (2016) 26936-26940.

[32] E. Jamroz, K. Kocot, B. Zawisza, E. Talik, A. Gagor, R. Sitko, A green analytical method for ultratrace determination of hexavalent chromium ions based on micro-solid phase extraction using amino-silanized cellulose membranes, Microchem. J. 149 (2019) 104060.

[33] Y. Li, H. Xiao, Y. Pan, M. Zhang, Y. Jin, Thermal and pH dual-responsive cellulose microfilament spheres for dye removal in single and binary systems, J. Hazard. Mater. 377 (2019) 88-97.

[34] U. Habiba, A.M. Afifi, A. Salleh, B.C. Ang, Chitosan/(polyvinyl alcohol)/zeolite electrospun composite nanofibrous membrane for adsorption of Cr^{6+}, Fe^{3+} and Ni^{2+}, J. Hazard. Mater. 322 (2017) 182-194.

[35] X. Yao, L. Guo, X. Chen, J. Huang, M. Steinhart, Y. Wang, Filtration-based synthesis of micelle-derived composite membranes for high-flux ultrafiltration, ACS

Appl. Mater. Interfaces 7 (2015) 6974-6981.

[36] A.H. Bahremand, S.M. Mousavi, A. Ahmadpour, M. Taherian, Biodegradable blend membranes of poly (butylene succinate)/cellulose acetate/dextran: preparation, characterization and performance, Carbohydr. Polym. 173 (2017) 497-507.

[37] Y. Li, Y. Wen, L. Wang, J. He, S.S. Al-Deyab, M. El-Newehy, J. Yu, B. Ding, Simultaneous visual detection and removal of lead(II) ions with pyromellitic dianhydride-grafted cellulose nanofibrous membranes, J. Mater. Chem. A 3 (2015) 18180-18189.

[38] X. Wang, Q. Zhang, C. Nam, M. Hickner, M. Mahoney, M.E. Meyerhoff, An ionophore-based anion-selective optode printed on cellulose paper, Angew. Chem. Int. Ed. 56 (2017) 11826-11830.

[39] G. Saikia, A.K. Dwivedi, P.K. Iyer, Development of solution, film and membrane based fluorescent sensor for the detection of fluoride anions from water, Anal. Methods 4 (2012) 3180-3186.

[40] Z. Li, H. Li, H. Xia, X. Ding, X. Luo, X. Liu, Y. Mu, Triarylboron-linked conjugated microporous polymers: sensing and removal of fluoride ions, Chem. Eur. J. 21 (2015) 17355-17362.

[41] C. Guizard, A. Bac, M. Barboiu, N. Hovnanian, Hybrid organic-inorganic membranes with specific transport properties: applications in separation and sensors technologies, Sep. Purif. Technol. 25 (2001) 167-180.

[42] K. Velmurugan, J. Prabhu, L. Tang, T. Chidambaram, M. Noel, S. Radhakrishnan,

R. Nandhakumar, A simple chalcone-based fluorescent chemosensor for the detection and removal of Fe^{3+} ions using a membrane separation method, Anal. Methods 6 (2014) 2883-2888.

[43] H.C. Wang, H. Zhou, B. Chen, P.M. Mendes, J.S. Fossey, T.D. James, Y.T. Long, A bis-boronic acid modified electrode for the sensitive and selective determination of glucose concentrations, Analyst 138 (2013) 7146-7151.

[44] G. Kyriakopoulos, D. Doulia, Adsorption of pesticides on carbonaceous and polymeric materials from aqueous solutions: a review, Sep. Purif. Rev. 35 (2006) 97-191.

[45] Y. Kim, G. Jang, T.S. Lee, New fluorescent metal-ion detection using a paper-based sensor strip containing tethered rhodamine carbon nanodots, ACS Appl. Mater. Interfaces 7 (2015) 15649-15657.

[46] R. Purbia, S. Paria, A simple turn on fluorescent sensor for the selective detection of thiamine using coconut water derived luminescent carbon dots, Biosens. Bioelectron. 79 (2016) 467-475.

[47] K. Shao, Y. Yang, S. Ye, D. Gu, T. Wang, Y. Teng, Z. Shen, Z. Pan, Dual-colored carbon dots-based ratiometric fluorescent sensor for high-precision detection of alkaline phosphatase activity, Talanta 208 (2020) 120460.

[48] L. Bao, Z.L. Zhang, Z.Q. Tian, L. Zhang, C. Liu, Y. Lin, B. Qi, D.W. Pang, Electrochemical tuning of luminescent carbon nanodots: from preparation to luminescence mechanism, Adv. Mater. 23 (2011) 5801-5806.

[49] B. van Dam, H. Nie, B. Ju, E. Marino, J.M.J. Paulusse, P. Schall, M. Li, K. Dohnalová, Excitation-dependent photoluminescence from single-carbon dots, Small 13 (2017) 1702098.

[50] P.H.F. Pereira, H.J.C. Voorwald, M.O.H. Cioffi, M.L.C.P. Da Silva, A.M.B. Rego, A.M. Ferraria, M.N. De Pinho, Sugarcane bagasse cellulose fibres and their hydrous niobium phosphate composites: synthesis and characterization by XPS, XRD and SEM, Cellulose 21 (2014) 641-652.

[51] M. Li, X. Li, X. An, Z. Chen, H. Xiao, Clustering-triggered emission of carboxymethylated nanocellulose, Front. Chem. 7 (2019) 447.

[52] L. Zheng, S. Zhang, W. Cheng, L. Zhang, P. Meng, T. Zhang, H. Yu, D. Peng, Theoretical calculations, molecular dynamics simulations and experimental investigation of the adsorption of cadmium(II) on amidoxime-chelating cellulose, J. Mater. Chem. A 7 (2019) 13714-13726.

[53] Z. Huang, Z. Huang, L. Feng, X. Luo, P. Wu, L. Cui, X. Mao, Modified cellulose by polyethyleneimine and ethylenediamine with induced Cu(II) and Pb(II) adsorption potentialities, Carbohydr. Polym. 202 (2018) 470-478.

[54] Y. Wu, Y. Jiang, Y. Li, R. Wang, Optimum synthesis of an amino functionalized microcrystalline cellulose from corn stalk for removal of aqueous Cu^{2+}, Cellulose 26 (2018) 805-821.

[55] H. Wang, B. Wang, Y. Bian, L. Dai, Enhancing photocatalytic activity of graphitic carbon nitride by codoping with P and C for efficient hydrogen generation,

ACS Appl. Mater. Interfaces 9 (2017) 21730-21737.

[56] Y. Qu, Y. Wu, Y. Gao, S. Qu, L. Yang, J. Hua, Diketopyrrolopyrrole-based fluorescent conjugated polymer for application of sensing fluoride ion and bioimaging, Sens. Actuators, B 197 (2014) 13-19.

[57] Y. Shen, X. Zhang, Y. Zhang, H. Li, Y. Chen, An ICT-Modulated strategy to construct colorimetric and ratiometric fluorescent sensor for mitochondria-targeted fluoride ion in cell living, Sensor. Actuat, B-Chem 258 (2018) 544-549.

[58] X. Lian, B. Yan, A postsynthetically modified MOF hybrid as a ratiometric fluorescent sensor for anion recognition and detection, Dalton Trans. 45 (2016) 18668-18675.

[59] L. Tang, M. Cai, P. Zhou, J. Zhao, K. Zhong, S. Hou, Y. Bian, A highly selective and ratiometric fluorescent sensor for relay recognition of zinc(II) and sulfide ions based on modulation of excited-state intramolecular proton transfer, RSC Adv. 3 (2013) 16802-16809.

[60] B. Gu, C. Dong, R. Shen, J. Qiang, T. Wei, F. Wang, S. Lu, X. Chen, Dioxetane-based chemiluminescent probe for fluoride ion-sensing in aqueous solution and living imaging, Sensor. Actuat, B-Chem 301 (2019) 127111.

[61] D. Dai, Z. Li, J. Yang, C. Wang, J.R. Wu, Y. Wang, D. Zhang, Y.W. Yang, Supramolecular assembly-induced emission enhancement for efficient mercury(II) detection and removal, J. Am. Chem. Soc. 141 (2019) 4756-4763.

[62] S. Wang, H. Ding, Y. Wang, C. Fan, G. Liu, S. Pu, A colorimetric and ratiometric

fluorescent sensor for sequentially detecting Cu^{2+} and arginine based on a coumarin–rhodamine B derivative and its application for bioimaging, RSC Adv. 9 (2019) 6643-6649.

[63] X. Hou, Y. Li, Y. Pan, Y. Jin, H. Xiao, Controlled release of agrochemicals and heavy metal ion capture dual-functional redox-responsive hydrogel for soil remediation, Chem. Commun. 54 (2018) 13714-13717.

[64] F. Wang, Y. Pan, P. Cai, T. Guo, H. Xiao, Single and binary adsorption of heavy metal ions from aqueous solutions using sugarcane cellulose-based adsorbent, Bioresour. Technol. 241 (2017) 482-490.

[65] M. Lan, J. Zhang, Y.-S. Chui, P. Wang, X. Chen, C.-S. Lee, H.-L. Kwong, W. Zhang, Carbon nanoparticle-based ratiometric fluorescent sensor for detecting mercury ions in aqueous media and living cells, ACS Appl. Mater. Interfaces 6 (2014) 21270-21278.

[66] M. Dhanushkodi, G.G. Vinoth Kumar, B.K. Balachandar, S. Sarveswari, S. Gandhi, J. Rajesh, A simple pyrazine based ratiometric fluorescent sensor for Ni^{2+} ion detection, Dyes Pigments 173 (2020) 107897.

[67] Y. Tian, M. Wu, R. Liu, D. Wang, X. Lin, W. Liu, L. Ma, Y. Li, Y. Huang, Modified native cellulose fibers-a novel efficient adsorbent for both fluoride and arsenic, J. Hazard. Mater. 185 (2011) 93-100.

[68] J. Zhang, N. Chen, P. Su, M. Li, C. Feng, Fluoride removal from aqueous solution by zirconium-chitosan/graphene oxide membrane, React. Funct. Polym. 114

(2017) 127-135.

[69] S.M. Prabhu, N. Viswanathan, S. Meenakshi, Defluoridation of water using chitosan assisted ethylenediamine functionalized synthetic polymeric blends, Int. J. Biol. Macromol. 70 (2014) 621-627.

[70] N. Gogoi, M. Barooah, G. Majumdar, D. Chowdhury, Carbon dots rooted agarose hydrogel hybrid platform for optical detection and separation of heavy metal ions, ACS Appl. Mater. Interfaces 7 (2015) 3058-3067.

[71] Z. Zhao, H. Chen, H. Zhang, L. Ma, Z. Wang, Polyacrylamide-phytic acid-polydopamine conducting porous hydrogel for rapid detection and removal of copper (II) ions, Biosens. Bioelectron. 91 (2017) 306-312.

[72] K. Im, D.N. Nguyen, S. Kim, H.J. Kong, Y. Kim, C.S. Park, O.S. Kwon, H. Yoon, Graphene-embedded hydrogel nanofibers for detection and removal of aqueous-phase dyes, ACS Appl. Mater. Interfaces 9 (2017) 10768-10776.